atoms

MDPI

Article

Calculated Transition Probabilities for Os VI Spectral Lines of Interest to Nuclear Fusion Research

Maxime Brasseur [1], Patrick Palmeri [1] and Pascal Quinet [1,2,*]

[1] Physique Atomique et Astrophysique, Université de Mons, B-7000 Mons, Belgium; maxime.brasseur@umons.ac.be (M.B.); patrick.palmeri@umons.ac.be (P.P.)
[2] IPNAS, Université de Liège, B-4000 Liège, Belgium
* Correspondence: pascal.quinet@umons.ac.be; Tel.: +32-65-37-36-29

Abstract: In this work, we present a new set of transition probabilities for experimentally classified spectral lines in the Os VI spectrum. To do this, two independent computational approaches based on the pseudo-relativistic Hartree–Fock, including core polarization effects (HFR+CPOL) and fully relativistic Multiconfiguration Dirac–Hartree–Fock (MCDHF) methods, were used, with the detailed comparison of the results obtained with these two approaches allowing us to estimate the quality of the calculated radiative parameters. These atomic data, corresponding to 367 lines of five-times ionized osmium between 438.720 and 1486.275 Å, are expected to be useful for the analysis of the spectra emitted by fusion plasmas in which osmium could appear as a result of transmutation by the neutron bombardment of tungsten used as component of the reactor wall, such as the ITER divertor.

Keywords: atomic data; transition probabilities; fusion plasma diagnostics

1. Introduction

It is now well established that tungsten (W) will be widely used in nuclear fusion reactors as a plasma-facing material due to its high melting point, low sputtering yield, and resistance to neutron irradiation. In particular, tungsten will be a key material for the divertor of the International Thermonuclear Experimental Reactor (ITER), the component designed to manage heat and particle flux from the plasma [1–3]. During nuclear fusion operations, the divertor will endure some of the harshest conditions in the reactor. Thus, under neutron bombardment, tungsten will undergo nuclear transmutation, forming other elements, including osmium [4].

As a transmutation product of tungsten, osmium atoms will also be sprayed into the plasma, altering its composition. Monitoring osmium's spectroscopic signals will help in understanding the dynamics of plasma–wall interactions, which are crucial for predicting material erosion and plasma contamination. The high ionization potential of neutral osmium (8.4 eV) means its ionic species may survive in high-temperature plasmas, providing diagnostic data about plasma conditions. Spectral lines of Os ions will therefore be particularly useful for identifying impurity influx from plasma-facing components, and the corresponding radiative decay rates will also be used to calculate essential plasma properties, such as electron temperature and density. These properties are actually mainly estimated by measuring intensity ratios between spectral lines emitted by the plasma (see, e.g., [5]). Since these intensities are proportional to the transition probabilities, these latter parameters are of paramount importance for plasma diagnostics.

The main goal of the present work is to make a new contribution to this field by determining the transition probabilities for spectral lines of five-times ionized osmium (Os

check for updates

Academic Editor: Karol Kozioł

Received: 23 December 2024
Revised: 17 January 2025
Accepted: 20 January 2025
Published: 21 January 2025

Citation: Brasseur, M.; Palmeri, P.; Quinet, P. Calculated Transition Probabilities for Os VI Spectral Lines of Interest to Nuclear Fusion Research. *Atoms* **2025**, *13*, 11. https://doi.org/10.3390/atoms13020011

Copyright: © 2025 by the authors. Licensee MDPI, Basel, Switzerland. This article is an open access article distributed under the terms and conditions of the Creative Commons Attribution (CC BY) license (https://creativecommons.org/licenses/by/4.0/).

VI), which is characterized by a moderately complex atomic structure with 71 electrons giving $5d^3\ {}^4F_{3/2}$ as the ground level. Spectroscopic studies have already been carried out previously for this ion. Indeed, nearly 30 years ago, Raassen et al. [6] classified 290 lines belonging to the $5d^3$–$5d^26p$ transition array in the 435–765 Å region and 87 lines belonging to the $5d^26s$–$5d^26p$ transition array in the 940–1510 Å region from the analysis of spectrograms made by means of the 3.0 m and 10.6 m normal incidence spectrographs installed at that time in Antigonish (Canada) and Meudon (France). This resulted in the determination of all levels (19) in the $5d^3$ ground configuration, 14 levels (out of 16 possible) in the $5d^26s$ configuration, and all levels (45) in the $5d^26p$ configuration. The analysis was guided by predicted energy level values and transition probabilities calculated by means of a complete set of orthogonal operators. Calculated energy values, *LS*-compositions, and *gA*-values, obtained from the fitted parameters using a rather limited configuration interaction, model were also reported. More recently, Azarov [7] critically reviewed the data available on the $5d^3$, $5d^26s$, and $5d^26p$ configurations in the Lu I isoelectronic sequence, including Os VI, by means of calculations with orthogonal operators. This study allowed for the determination of two new levels in the $5d^26s$ configuration of Os VI, namely $(^3P)^2P_{1/2}$ and $(^3P)^4P_{5/2}$.

If the electronic structure of the first three configurations of Os VI is now well known, the same cannot be said for the radiative parameters, which have only been calculated by means of the pseudo-relativistic Hartree–Fock method (HFR) including the configuration interaction in a very limited way [6]. This motivated the present work, the objective of which is to provide a new set of reliable transition probabilities for experimentally observed spectral lines of Os VI. To do this, two independent methods were used, namely the pseudo-relativistic Hartree–Fock approach including core polarization corrections (HFR+CPOL) and the fully relativistic Multiconfiguration Dirac–Hartree–Fock approach (MCDHF), with the cross-comparison of the results obtained with these two methods allowing us to estimate the accuracy of the new calculated radiative data.

2. Computational Approaches

2.1. Pseudo-Relativistic Hartree–Fock Method with Core Polarization Corrections

The first method used for computing the radiative rates in Os VI was the pseudo-relativistic Hartree–Fock (HFR) method, originally introduced by Cowan [8], modified for taking core polarization effects into account, giving rise to the so-called HFR+CPOL method, as described, e.g., in [9–11].

The physical model was chosen as consisting of three valence electrons surrounding an Os IX-type ionic core with 68 electrons. This led us to consider the valence–valence interactions by explicitly introducing the following configurations into the calculations: $5d^3$ + $5d^26s$ + $5d^27s$ + $5d6s^2$ + $5d^26d$ + $5d6p^2$ + $5d6d^2$ + $5d5f^2$ + $5d6f^2$ + $5d6s6d$ + $5d6p5f$ + $5d6p6f$ + $5d5f6f$ + $6s^26d$ + $6s6p^2$ + $6p^26d$ + $6s6d^2$ + $6d^3$ + $6s5f^2$ + $6d5f^2$ + $6s6f^2$ + $6d6f^2$ for the even parity, and $5d^26p$ + $5d^27p$ + $5d^25f$ + $5d^26f$ + $5d6s6p$ + $5d6s5f$ + $5d6s6f$ + $5d6p6d$ + $5d6d5f$ + $5d6d6f$ + $6s^26p$ + $6s^25f$ + $6s^26f$ + $6p^25f$ + $6p^26f$ + $6p^3$ + $6p6d^2$ + $6d^25f$ + $6d^26f$ + $6p5f^2$ + $6p6f^2$ + $5f^26f$ + $5f6f^2$ for the odd parity. This list of configurations is similar to the one considered for our recent HFR+CPOL calculations of radiative parameters in the isoelectronic ion Re V [12], to which the $5d^27s$ and $5d^27p$ configurations were added. Core–valence interactions were then estimated using a core polarization potential and a correction to the electric dipole operator, as described in [9–11], with a dipole polarizability α_d = 1.50 $a_0{}^3$ and a cut-off radius r_c = 1.12 a_0, the former parameter being found by extrapolating the α_d-values published by Fraga et al. [13] for the first ions of the erbium isoelectronic sequence, i.e., Tm II, Yb III, Lu IV, and Hf V, while the latter parameter corresponds to the mean radius of the outermost orbital of the Os IX ionic core (5p), as obtained in the HFR calculations.

It should be noted that this HFR+CPOL approach is valid if core-excited configurations do not overlap the configurations of interest. It was verified that this is actually the case for the $5d^3$, $5d^26s$, and $5d^26p$ configurations in Os VI. Indeed, a simple calculation of average energies for some configurations with an electron excitation from the 4f and 5p core orbitals showed that such configurations were located well above the $5d^3$, $5d^26s$ and $5d^26p$ configurations in Os VI. This is illustrated in Figure 1 where the average energies of the $5p^55d^4$, $5p^55d^36s$, $5p^55d^36p$, and $4f^{13}5d^4$ core-excited configurations are compared with those corresponding to the $5d^3$, $5d^26s$, and $5d^26p$ configurations along the Lu isoelectronic sequence from Ta III to Ra XVIII. When looking at this figure, it is clear that the lowest configurations with open 5p and 4f orbitals are several hundred thousand cm^{-1} above the $5d^3$, $5d^26s$, and $5d^26p$ configurations in Os VI (Z_c = 6). Their interactions with the latter can therefore be estimated by means of the CPOL effects introduced in the HFR method. It is also interesting to note that this is no longer the case for higher ionization stages in the isoelectronic sequence since the $5p^55d^4$ and $5d^36p$ configurations cross each other around At XV (Z_c = 15). For neighboring and higher charged ions, it would then be necessary to explicitly introduce the $5p^55d^4$ configuration in the calculations rather than estimating its influence on the $5d^3$–$5d^26p$ and $5d^26s$–$5d^26p$ transitions by means of CPOL corrections.

The HFR+CPOL calculations were then refined using a well-known least-squares fitting procedure of the computed energy levels to the experimental values available in the literature. More precisely, the experimental energy levels belonging to the $5d^3$ and $5d^26s$ even configurations and the $5d^26p$ odd configuration published by Raassen et al. [6] were used to optimize the radial parameters corresponding to the average energies (E_{av}), the Slater integrals (F^k, G^k, R^k), the spin orbit parameters (ζ_{nl}), and the effective interaction parameters α and β characterizing these three configurations. This led to average deviations between calculated and experimental energies of 46 cm^{-1} and 150 cm^{-1} for the even and odd parities, respectively. These deviations are slightly higher than those obtained in the fits made by Raaseen et al. [6] (i.e., 11 and 107 cm^{-1}) and Azarov [7] (14 and 95 cm^{-1}) for the same configurations, but it should be noted that our calculations include a much larger number of interacting configurations, which often leads to slightly more complicated adjustment procedures because of the more numerous mixtures in the eigenvector compositions. A detailed comparison between the HFR+CPOL levels and the available experimental values reported in [6,7] is given in Table 1, in which the first two *LS*-components obtained in our calculations for each level are also listed. These eigenvector compositions are in excellent agreement with those published in [7].

2.2. Fully Relativistic Multiconfiguration Dirac–Hartree–Fock Method

The second computational approach used in the present work was the fully relativistic Multiconfiguration Dirac–Hartree–Fock (MCDHF) method, as described in [14,15] and implemented in the latest version of the General Relativistic Atomic Structure Package, namely GRASP2018 [16].

We started our calculations by considering the $5d^3$ and $5d^26s$ even and the $5d^26p$ odd parity configurations as the multireference (MR) with all the orbitals optimized on the $5d^3\,{}^4F_{3/2}$ ground state, in a first step, and then optimizing separately only the 5d and 6s orbitals on all the levels of the MR even configurations ($5d^3$ + $5d^26s$), and only the 5d and 6p orbitals on all the levels of the MR odd configuration $5d^26p$. Thereafter, correlation orbitals were introduced and optimized layer by layer on all the levels of the MR in two steps in valence–valence (VV) expansions of the atomic state functions (ASFs), where all single and double (SD) excitations were allowed from the 5d, 6s, and 6p spectroscopic orbitals to the following orbital active sets (ASs), where the set of n_{max} stands for the maximum value of the orbital principal quantum number for each azimuthal quantum number *l*: {7s,6p,6d,5f}

and {6s,7p,6d,5f} for the even and odd parities, respectively, in a first step (VV1 model), and {8s,7p,7d,6f} and {7s,8p,7d,6f} for the even and odd parities, respectively, in a second step (VV2 model). Finally, core–valence (CV) and core–core (CC) correlations were considered in a relativistic configuration interaction (RCI) calculation using the orbitals optimized previously. Here, the ASF expansions were further extended by adding SD excitations from the 4f core orbital of the MR configurations to the AS of the last step of the orbital optimizations. This gave rise to 515,057 and 900,402 configuration state functions (CSFs) in the even and odd parities, respectively.

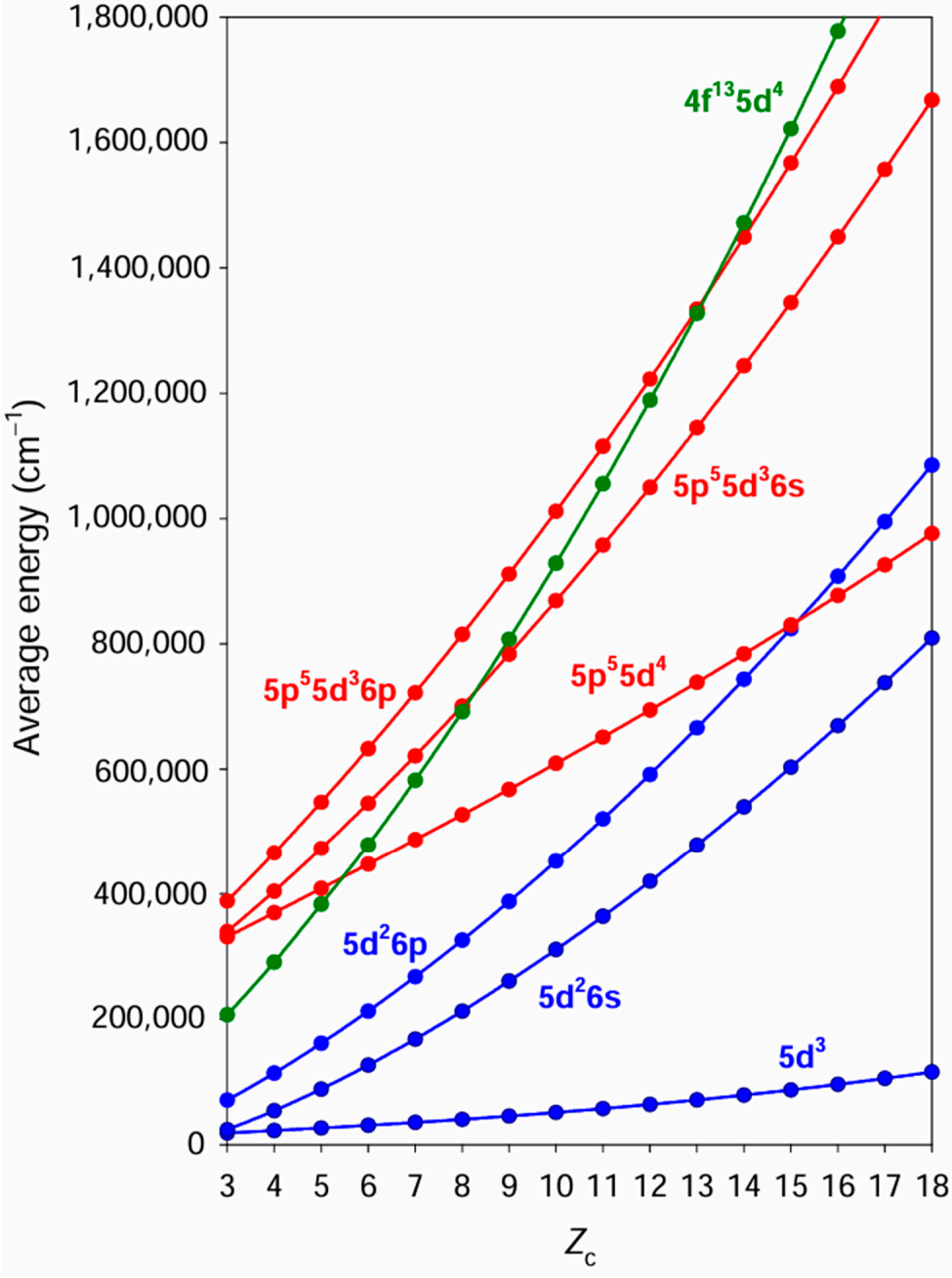


Figure 1. Average energies obtained with the HFR+CPOL method for $5d^3$, $5d^26s$, $5d^26p$, $5p^55d^4$, $5p^55d^36s$, $5p^55d^36p$, and $4f^{13}5d^4$ configurations in Lu-like ions from Ta III (Z_c = 3) to Ra XVIII (Z_c = 18). $Z_c = Z - N + 1$, where Z is the atomic number and N is the total number of electrons in the ion.

Table 1. Comparison of the energy levels computed in the present work using the HFR+CPOL and MCDHF methods with the available experimental values for the $5d^3$, $5d^26s$, and $5d^26p$ configurations of Os VI. All values are given in cm^{-1}.

Conf.	Composition [1]	J	E_{EXP} [2]	$E_{HFR+CPOL}$	$\Delta E_{HFR+CPOL}$	E_{MCDHF}	ΔE_{MCDHF}
$5d^3$	81% ^{4}F + 10% ^{2}D	1.5	0.0	0	0	0	0
	94% ^{4}F + 4% ^{2}D	2.5	6397.4	6422	25	5912	−485
	84% ^{4}F + 13% ^{2}G	3.5	11,444.1	11,450	6	11,045	−399
	46% ^{4}P + 35% ^{2}P	1.5	14,430.2	14,390	−40	15,525	1095
	56% ^{4}F + 33% ^{2}G	4.5	14,678.3	14,651	−27	14,901	223
	68% ^{4}P + 32% ^{2}P	0.5	16,772.4	16,806	34	17,878	1106
	81% ^{2}G + 15% ^{4}F	3.5	22,919.6	22,950	30	24,181	1261
	56% ^{2}H + 34% ^{4}F	4.5	24,028.4	24,054	26	25,420	1392
	89% ^{4}P + 7% ^{2}D	2.5	24,828.5	24,808	−20	25,636	808
	42% ^{4}P + 34% ^{2}D	1.5	27,894.0	27,944	50	28,591	697
	67% ^{2}P + 32% ^{4}P	0.5	28,859.8	28,876	16	29,696	836
	100% ^{2}H	5.5	32,155.8	32,159	3	34,620	2464
	84% ^{2}D + 6% ^{2}D	2.5	34,417.8	34,433	15	35,784	1366
	57% ^{2}G + 32% ^{2}H	4.5	37,019.4	37,011	−8	38,308	1289
	85% ^{2}F + 8% ^{2}D	2.5	39,600.8	39,572	−29	43,286	3685
	55% ^{2}P + 17% ^{2}D	1.5	40,202.6	40,186	−17	40,607	404
	94% ^{2}F + 5% ^{2}G	3.5	40,447.0	40,455	8	43,864	3417
	66% ^{2}D + 33% ^{2}D	1.5	59,910.8	59,972	61	63,816	4005
	77% ^{2}D + 12% ^{2}F	2.5	61,005.3	60,968	−37	64,058	3053
$5d^26s$	91% (^{3}F)^{4}F + 8% (^{1}D)^{2}D	1.5	97,940.4	97,929	−11	101,568	3628
	78% (^{3}F)^{4}F + 12% (^{3}F)^{2}F	2.5	100,973.9	101,053	79	104,606	3632
	95% (^{3}F)^{4}F + 5% (^{3}F)^{2}F	3.5	108,538.4	108,578	40	111,778	3240
	53% (^{3}F)^{2}F + 21% (^{3}F)^{4}F	2.5	114,140.1	114,133	−7	118,083	3943
	90% (^{3}P)^{4}P + 7% (^{1}S)^{2}S	0.5	114,363.2	114,318	−45	119,157	4794
	90% (^{3}F)^{4}F + 10% (^{1}G)^{2}G	4.5	115,173.8	115,184	10	118,469	3295
	85% (^{3}P)^{4}P + 12% (^{1}D)^{2}D	1.5	118,499.8	118,478	−22	123,014	4514
	51% (^{3}P)^{4}P + 29% (^{3}F)^{2}F	2.5	119,205.3	119,259	54	123,539	4334
	59% (^{1}D)^{2}D + 21% (^{3}P)^{2}P	1.5	123,318.6	123,334	15	128,060	4741
	61% (^{3}F)^{2}F + 36% (^{1}G)^{2}G	3.5	123,600.5	123,520	−80	128,038	4438
	90% (^{3}P)^{2}P + 5% (^{3}P)^{4}P	0.5	129,179.2	129,417	238	134,405	5226
	89% (^{1}G)^{2}G + 10% (^{3}F)^{4}F	4.5	130,849.6	130,957	107	136,556	5706
	55% (^{1}D)^{2}D + 39% (^{3}P)^{4}P	2.5	131,676.2	131,632	−44	135,923	4247
	63% (^{1}G)^{2}G + 33% (^{3}F)^{2}F	3.5	132,989.9	132,897	−93	138,231	5241
	77% (^{3}P)^{2}P + 19% (^{1}D)^{2}D	1.5	138,441.2	138,555	114	143,272	4831
	89% (^{1}S)^{2}S + 5% (^{3}P)^{2}P	0.5	157,388.9	157,398	8	162,297	4907
$5d^26p$	62% (^{3}F)^{4}G + 19% (^{3}F)^{2}F	2.5	170,473.6	170,724	250	194,287	23,813
	48% (^{3}F)^{4}F + 31% (^{3}F)^{2}D	1.5	175,839.8	175,579	−261	199,974	24,134
	72% (^{3}F)^{4}G + 11% (^{3}F)^{2}F	3.5	182,479.5	182,524	44	205,881	23,401
	44% (^{3}F)^{4}F + 20% (^{3}F)^{2}D	2.5	184,033.0	184,198	165	207,833	23,800
	50% (^{3}P)^{4}D + 16% (^{3}P)^{2}S	0.5	186,854.0	186,757	−97	211,679	24,825

Table 1. *Cont.*

Conf.	Composition [1]	J	E_{EXP} [2]	$E_{HFR+CPOL}$	$\Delta E_{HFR+CPOL}$	E_{MCDHF}	ΔE_{MCDHF}
	36% $(^3F)^4G$ + 21% $(^3F)^4F$	4.5	190,882.5	190,866	−17	214,816	23,933
	27% $(^3P)^4D$ + 21% $(^1D)^2P$	1.5	190,987.8	191,141	153	215,754	24,766
	20% $(^3F)^4G$ + 13% $(^3P)^4D$	2.5	191,516.9	191,381	−136	215,489	23,972
	39% $(^3P)^2S$ + 33% $(^3P)^4P$	0.5	192,087.9	192,468	380	216,865	24,777
	33% $(^3F)^4D$ + 31% $(^3F)^4F$	3.5	192,575.6	192,473	−103	216,520	23,944
	35% $(^3F)^4F$ + 18% $(^3F)^2D$	1.5	194,263.2	194,306	43	217,644	23,381
	39% $(^3P)^4D$ + 21% $(^3P)^4S$	1.5	195,716.1	195,276	−440	220,433	24,717
	24% $(^3F)^2F$ + 20% $(^3F)^4D$	2.5	196,152.8	196,100	−53	219,905	23,752
	33% $(^3F)^2G$ + 17% $(^3F)^4G$	3.5	197,134.0	197,161	27	220,461	23,327
	70% $(^3F)^4D$ + 13% $(^1D)^2P$	0.5	198,144.3	198,214	70	222,234	24,090
	57% $(^3F)^4G$ + 18% $(^1G)^2G$	4.5	202,263.2	202,190	−73	225,816	23,553
	46% $(^1G)^2G$ + 29% $(^3F)^4F$	3.5	203,069.9	203,306	236	227,580	24,510
	18% $(^3F)^2F$ + 18% $(^1D)^2F$	2.5	204,720.9	204,779	58	228,186	23,465
	38% $(^3P)^4S$ + 20% $(^1D)^2P$	1.5	205,711.8	205,702	−10	230,358	24,646
	20% $(^3F)^2G$ + 18% $(^3F)^2F$	3.5	206,193.4	206,188	−5	230,443	24,250
	41% $(^3F)^4F$ + 34% $(^1G)^2H$	4.5	206,555.3	206,346	−209	231,212	24,657
	29% $(^3F)^2F$ + 28% $(^1D)^2F$	2.5	207,333.9	207,247	−87	231,344	24,010
	55% $(^3F)^4D$ + 20% $(^3F)^2D$	1.5	207,349.5	207,473	123	230,967	23,617
	25% $(^3F)^4D$ + 17% $(^3P)^4D$	3.5	209,856.0	209,916	60	233,316	23,460
	90% $(^3F)^4G$ + 10% $(^1G)^2H$	5.5	210,146.1	209,870	−276	232,910	22,764
	60% $(^3P)^4P$ + 14% $(^3P)^4S$	1.5	211,634.7	211,444	−191	236,166	24,531
	39% $(^3P)^4P$ + 28% $(^1D)^2P$	0.5	212,086.5	212,047	−40	236,322	24,235
	25% $(^3P)^4D$ + 25% $(^3F)^2D$	2.5	214,387.4	214,508	121	238,266	23,879
	55% $(^3F)^2G$ + 21% $(^3F)^4F$	4.5	215,369.6	215,554	214	238,802	23,432
	42% $(^3P)^4P$ + 27% $(^1D)^2D$	2.5	216,397.1	216,259	−138	240,712	24,315
	33% $(^3P)^4D$ + 16% $(^3F)^4D$	3.5	216,704.6	216,785	80	240,859	24,154
	30% $(^1D)^2D$ + 27% $(^3P)^2P$	1.5	217,361.9	217,482	120	241,850	24,488
	53% $(^3P)^2D$ + 14% $(^3F)^2D$	1.5	219,500.4	219,622	122	244,276	24,776
	36% $(^1D)^2P$ + 20% $(^3P)^4P$	0.5	219,979.0	219,971	−8	244,249	24,270
	24% $(^1D)^2D$ + 23% $(^3F)^2D$	2.5	220,744.9	220,682	−63	245,292	24,547
	42% $(^1G)^2G$ + 33% $(^1G)^2H$	4.5	221,932.2	221,965	33	246,907	24,975
	42% $(^3P)^2P$ + 30% $(^1S)^2P$	0.5	224,004.9	224,156	151	248,952	24,947
	41% $(^1D)^2F$ + 33% $(^3P)^4D$	3.5	225,818.9	225,920	101	249,663	23,844
	89% $(^1G)^2H$ + 10% $(^3F)^4G$	5.5	226,320.5	226,170	−150	251,706	25,386
	33% $(^1G)^2F$ + 18% $(^3P)^2D$	2.5	227,935.6	228,019	83	252,758	24,822
	47% $(^1G)^2F$ + 20% $(^1G)^2G$	3.5	228,256.2	228,274	18	253798	25,542
	48% $(^3P)^2P$ + 16% $(^1D)^2D$	1.5	231,998.6	231,890	−109	256680	24,681
	55% $(^1G)^2F$ + 15% $(^3F)^2D$	2.5	233,168.5	233,242	74	258815	25,647
	53% $(^1S)^2P$ + 26% $(^3P)^2P$	0.5	236,614.5	236,645	31	262090	25,476
	87% $(^1S)^2P$ + 3% $(^3P)^2D$	1.5	252,203.4	252,163	−40	277153	24,950

[1] Only the first two components, as computed in our HFR+CPOL model, are given. [2] Experimental energy level values taken from [6,7].

The final MCDHF energy levels are compared to the available experimental values in Table 1, where it can be seen that a satisfactory agreement has been reached, the average deviation being equal to 8% for the whole set of energy levels belonging to the $5d^3$, $5d^26s$, and $5d^26p$ configurations, with a lower value for even parity levels (4%) compared to the value obtained for odd parity levels (10%). It would be necessary to extend the orbital active sets to see if a better agreement between the MCDHF and experimental levels could be obtained, but as the main purpose of the MCDHF calculations was to verify the overall consistency of the HFR+CPOL radiative parameters, we preferred not to run more extended (and time-consuming) MCDHF calculations in the present work.

3. Radiative Decay Rates

Transition probabilities (gA in 10^{10} s^{-1}) obtained in the present work with the HFR+CPOL and MCDHF methods are reported in Table 2. They are given for the lines experimentally identified by Raassen et al. [6] in the Os VI spectrum between 438.720 and 1486.275 Å. In this table, the transitions are classified by the numerical values of the lower and upper energy levels, with the spectroscopic designations of these levels given in Table 1. Transition probabilities published in [6] are also given for comparison in Table 2.

Table 2. Transition probabilities for experimentally observed lines in the Os VI emission spectrum.

λ (Å) [1]	Lower Level [2]		Upper Level [2]		gA (10^{10} s^{-1})		
	E (cm^{-1})	J	E (cm^{-1})	J	Previous [3]	HFR+CPOL [4]	MCDHF [4]
438.720	0.0	1.5	227,935.6	2.5	0.006	0.006 *	0.004
455.577	0.0	1.5	219,500.4	1.5	0.068	0.062 *	0.042
459.160	34,417.8	2.5	252,203.4	1.5	0.150	0.159	0.220
461.913	11,444.1	3.5	227,935.6	2.5	0.022	0.025 *	0.022
466.531	6397.4	2.5	220,744.9	2.5	0.092	0.091	0.053
469.251	6397.4	2.5	219,500.4	1.5	0.017	0.025 *	0.024
471.499	0.0	1.5	212,086.5	0.5	0.025	0.024 *	0.022
471.694	40,202.6	1.5	252,203.4	1.5	0.185	0.302	0.275
472.510	0.0	1.5	211,634.7	1.5	0.069	0.071	0.044
473.616	14,678.3	4.5	225,818.9	3.5	0.061	0.072 *	0.148
474.010	6397.4	2.5	217,361.9	1.5	0.052	0.060 *	0.041
475.490	6397.4	2.5	216,704.6	3.5	0.007	0.011 *	0.012 **
475.625	22,919.6	3.5	233,168.5	2.5	0.104	0.104 *	0.126
476.191	6397.4	2.5	216,397.1	2.5	0.085	0.086 *	0.084
477.151	14,430.2	1.5	224,004.9	0.5	0.041	0.046 *	0.051
477.779	11,444.1	3.5	220,744.9	2.5	0.211	0.252	0.166
479.981	24,828.5	2.5	233,168.5	2.5	0.049	0.051 *	0.030 **
482.493	14,678.3	4.5	221,932.2	4.5	0.012	0.021 *	0.009 **
486.120	0.0	1.5	205,711.8	1.5	0.038	0.037 *	0.043
487.005	22,919.6	3.5	228,256.2	3.5	0.127	0.112 *	0.101
487.180	11,444.1	3.5	216,704.6	3.5	0.247	0.237	0.196
487.241	6397.4	2.5	211,634.7	1.5	0.054	0.068	0.035
487.643	14,430.2	1.5	219,500.4	1.5	0.049	0.065 *	0.042

Table 2. *Cont.*

λ (Å) [1]	Lower Level [2]		Upper Level [2]		gA (10^{10} s^{-1})		
	E (cm^{-1})	J	E (cm^{-1})	J	Previous [3]	HFR+CPOL [4]	MCDHF [4]
487.767	22,919.6	3.5	227,935.6	2.5	0.309	0.291	0.225
487.916	11,444.1	3.5	216,397.1	2.5	0.163	0.165	0.170
488.470	0.0	1.5	204,720.9	2.5	0.023	0.027 *	0.028 **
489.648	24,028.4	4.5	228,256.2	3.5	0.459	0.424	0.215
490.375	11,444.1	3.5	215,369.6	4.5	0.206	0.196	0.153
491.577	24,828.5	2.5	228,256.2	3.5	0.174	0.179	0.125 **
492.275	28,859.8	0.5	231,998.6	1.5	0.095	0.096 *	0.074
492.355	24,828.5	2.5	227,935.6	2.5	0.096	0.099 *	0.113
492.775	14,430.2	1.5	217,361.9	1.5	0.029	0.051 *	0.027
492.857	22,919.6	3.5	225,818.9	3.5	0.096	0.130 *	0.071
494.335	24,028.4	4.5	226,320.5	5.5	0.289	0.254	0.228
494.985	14,678.3	4.5	216,704.6	3.5	0.547	0.563 *	0.527
495.131	14,430.2	1.5	216,397.1	2.5	0.129	0.142	0.137
495.562	24,028.4	4.5	225,818.9	3.5	0.116	0.197 *	0.341
497.635	6397.4	2.5	207,349.5	1.5	0.162	0.152 *	0.057
497.671	6397.4	2.5	207,333.9	2.5	0.114	0.111	0.135
498.279	14,678.3	4.5	215,369.6	4.5	0.496	0.567	0.660
498.536	16,772.4	0.5	217,361.9	1.5	0.083	0.091	0.064
499.892	27,894.0	1.5	227,935.6	2.5	0.116	0.130 *	0.137
500.108	14,430.2	1.5	214,387.4	2.5	0.103	0.066 *	0.090
500.511	6397.4	2.5	206,193.4	3.5	0.141	0.166	0.027
502.478	22,919.6	3.5	221,932.2	4.5	0.078	0.099	0.047
503.144	34,417.8	2.5	233,168.5	2.5	0.187	0.210 *	0.090
504.230	6397.4	2.5	204,720.9	2.5	0.029	0.050 *	0.025
504.684	0.0	1.5	198,144.3	0.5	0.262	0.251	0.099 **
505.302	24,028.4	4.5	221,932.2	4.5	0.162	0.179 *	0.094
505.501	22,919.6	3.5	220,744.9	2.5	0.056	0.080 *	0.056
506.123	34,417.8	2.5	231,998.6	1.5	0.157	0.183 *	0.147
508.462	6397.4	2.5	203,069.9	3.5	0.188	0.148	0.228
509.134	40,202.6	1.5	236,614.5	0.5	0.038	0.078 *	0.033
509.800	0.0	1.5	196,152.8	2.5	0.050	0.052 *	0.010
509.914	27,894.0	1.5	224,004.9	0.5	0.507	0.542	0.524
510.425	24,828.5	2.5	220,744.9	2.5	0.123	0.163	0.137
510.492	11,444.1	3.5	207,333.9	2.5	0.312	0.388	0.423
510.947	0.0	1.5	195,716.1	1.5	0.130	0.129	0.184
511.593	14,678.3	4.5	210,146.1	5.5	0.758	0.678	0.749
512.354	14,678.3	4.5	209,856.0	3.5	0.414	0.474 *	0.805
512.442	28,859.8	0.5	224,004.9	0.5	0.061	0.065	0.108
512.534	11,444.1	3.5	206,555.3	4.5	0.035	0.029 *	0.074
513.482	11,444.1	3.5	206,193.4	3.5	0.588	0.687	0.319

Table 2. *Cont.*

λ (Å) [1]	Lower Level [2]		Upper Level [2]		gA (10^{10} s^{-1})		
	E (cm^{-1})	J	E (cm^{-1})	J	Previous [3]	HFR+CPOL [4]	MCDHF [4]
513.684	24,828.5	2.5	219,500.4	1.5	0.137	0.129	0.135
514.766	0.0	1.5	194,263.2	1.5	0.071	0.089 *	0.104 **
515.025	32,155.8	5.5	226,320.5	5.5	3.680	3.790	3.759
516.033	22,919.6	3.5	216,704.6	3.5	0.081	0.082 *	0.053
516.617	39,600.8	2.5	233,168.5	2.5	0.978	1.001	1.224
516.749	34,417.8	2.5	227,935.6	2.5	0.503	0.542	0.666
516.858	22,919.6	3.5	216,397.1	2.5	0.078	0.120	0.093
517.396	11,444.1	3.5	204,720.9	2.5	0.082	0.039 *	0.146 **
518.539	27,894.0	1.5	220,744.9	2.5	0.183	0.156 *	0.141
518.885	40,447.0	3.5	233,168.5	2.5	0.105	0.108 *	0.031
519.756	39,600.8	2.5	231,998.6	1.5	0.299	0.338	0.289
520.051	59,910.8	1.5	252,203.4	1.5	0.294	0.263	0.227
520.597	0.0	1.5	192,087.9	0.5	0.239	0.230	0.282
521.169	14,678.3	4.5	206,555.3	4.5	0.925	0.851	0.580
521.386	40,202.6	1.5	231,998.6	1.5	0.933	0.802	0.746
521.858	11,444.1	3.5	203,069.9	3.5	0.343	0.255	0.593
522.008	24,828.5	2.5	216,397.1	2.5	1.520	1.593	1.560
522.152	0.0	1.5	191,516.9	2.5	0.158	0.144	0.156
522.282	22,919.6	3.5	214,387.4	2.5	0.268	0.245	0.239
522.466	34,417.8	2.5	225,818.9	3.5	0.244	0.235	0.263
522.631	24,028.4	4.5	215,369.6	4.5	0.424	0.535	0.297 **
522.911	37,019.4	4.5	228,256.2	3.5	0.876	1.364	1.264
523.020	61,005.3	2.5	252,203.4	1.5	1.960	1.878	1.819
523.232	28,859.8	0.5	219,979.0	0.5	0.099	0.076 *	0.048
523.595	0.0	1.5	190,987.8	1.5	0.099	0.073 *	0.126
524.721	16,772.4	0.5	207,349.5	1.5	0.072	0.060 *	0.090
525.512	14,430.2	1.5	204,720.9	2.5	0.262	0.246	0.279
526.939	32,155.8	5.5	221,932.2	4.5	0.841	0.565	1.437
526.999	6397.4	2.5	196,152.8	2.5	0.038	0.103 *	0.0003
528.211	6397.4	2.5	195,716.1	1.5	1.060	1.287	0.907
529.270	16,772.4	0.5	205,711.8	1.5	0.132	0.116	0.120
529.661	37,019.4	4.5	225,818.9	3.5	7.410	6.775	6.104
530.070	39,600.8	2.5	228,256.2	3.5	0.074	0.084 *	0.078
530.507	28,859.8	0.5	217,361.9	1.5	0.024	0.018 *	0.017 **
530.811	14,678.3	4.5	203,069.9	3.5	0.501	0.348	0.241
530.969	39,600.8	2.5	227,935.6	2.5	0.472	0.469	0.230
532.296	6397.4	2.5	194,263.2	1.5	1.060	0.864	1.045
532.456	40,447.0	3.5	228,256.2	3.5	1.630	1.495	1.794
532.675	40,202.6	1.5	227,935.6	2.5	0.254	0.249	0.179 **
533.093	14,678.3	4.5	202,263.2	4.5	1.920	1.830	2.568

Table 2. *Cont.*

λ (Å) [1]	Lower Level [2]		Upper Level [2]		gA (10^{10} s^{-1})		
	E (cm^{-1})	J	E (cm^{-1})	J	Previous [3]	HFR+CPOL [4]	MCDHF [4]
533.367	40,447.0	3.5	227,935.6	2.5	0.654	0.701	0.849
535.179	0.0	1.5	186,854.0	0.5	1.240	1.210	1.448
535.318	24,828.5	2.5	211,634.7	1.5	1.950	1.804	1.887
536.215	27,894.0	1.5	214,387.4	2.5	0.236	0.266	0.289 **
536.691	34,417.8	2.5	220,744.9	2.5	0.098	0.053 *	0.143
537.011	39,600.8	2.5	225,818.9	3.5	0.023	0.020 *	0.018
537.119	6397.4	2.5	192,575.6	3.5	0.151	0.159	0.203
537.294	24,028.4	4.5	210,146.1	5.5	0.217	0.196	0.140 **
538.138	24,028.4	4.5	209,856.0	3.5	6.290	6.070	6.008
538.532	11,444.1	3.5	197,134.0	3.5	0.459	0.565	0.406
539.465	40,447.0	3.5	225,818.9	3.5	0.093	0.200	0.123
540.191	6397.4	2.5	191,516.9	2.5	1.560	1.344	1.583
540.457	24,828.5	2.5	209,856.0	3.5	0.280	0.204	0.271
540.795	37,019.4	4.5	221,932.2	4.5	4.350	4.338	3.921
541.393	11,444.1	3.5	196,152.8	2.5	4.690	4.279	4.746
541.741	6397.4	2.5	190,987.8	1.5	1.170	1.012	1.529
542.260	22,919.6	3.5	207,333.9	2.5	4.840	4.806	4.262
542.911	27,894.0	1.5	212,086.5	0.5	0.486	0.473	0.544
543.383	0.0	1.5	184,033.0	2.5	0.211	0.196	0.256
544.063	40,202.6	1.5	224,004.9	0.5	0.427	0.491	0.242
544.249	27,894.0	1.5	211,634.7	1.5	0.028	0.046 *	0.008
544.324	14,430.2	1.5	198,144.3	0.5	0.172	0.156	0.117
544.555	22,919.6	3.5	206,555.3	4.5	0.160	0.096 *	0.198
545.629	22,919.6	3.5	206,193.4	3.5	0.147	0.271	0.138
545.771	28,859.8	0.5	212,086.5	0.5	0.859	0.808	0.781
545.809	32,155.8	5.5	215,369.6	4.5	11.100	10.250	10.048
546.616	34,417.8	2.5	217,361.9	1.5	2.110	2.116	1.978
547.126	28,859.8	0.5	211,634.7	1.5	0.112	0.127	0.104
547.863	24,028.4	4.5	206,555.3	4.5	3.710	3.342	3.974
548.078	14,678.3	4.5	197,134.0	3.5	5.150	4.868	4.651
548.589	34,417.8	2.5	216,704.6	3.5	0.346	0.328	0.229
548.954	24,028.4	4.5	206,193.4	3.5	2.290	1.802	1.889
549.515	34,417.8	2.5	216,397.1	2.5	0.189	0.286	0.276
550.051	22,919.6	3.5	204,720.9	2.5	0.410	0.108 *	0.827
550.291	14,430.2	1.5	196,152.8	2.5	0.160	0.116 *	0.058
551.011	40,447.0	3.5	221,932.2	4.5	0.604	0.444	0.470
551.358	16,772.4	0.5	198,144.3	0.5	0.675	0.639	0.632
551.616	14,430.2	1.5	195,716.1	1.5	0.801	0.542	1.020
552.086	11,444.1	3.5	192,575.6	3.5	3.200	2.877	3.444
552.843	24,828.5	2.5	205,711.8	1.5	0.396	0.276	0.316

Table 2. *Cont.*

λ (Å) [1]	Lower Level [2]		Upper Level [2]		gA (10^{10} s^{-1})		
	E (cm^{-1})	J	E (cm^{-1})	J	Previous [3]	HFR+CPOL [4]	MCDHF [4]
553.893	40,202.6	1.5	220,744.9	2.5	0.635	0.579	0.484
554.642	40,447.0	3.5	220,744.9	2.5	6.130	2.891	3.099
555.091	22,919.6	3.5	203,069.9	3.5	3.530	3.246	3.614
555.333	11,444.1	3.5	191,516.9	2.5	0.117	0.246	0.014 **
555.652	34,417.8	2.5	214,387.4	2.5	1.820	1.410	1.336
555.870	39,600.8	2.5	219,500.4	1.5	2.580	2.434	2.650
556.072	14,430.2	1.5	194,263.2	1.5	1.150	1.159	0.785
556.247	40,202.6	1.5	219,979.0	0.5	1.240	1.067	1.429
556.528	37,019.4	4.5	216,704.6	3.5	1.100	0.938	1.503
557.245	27,894.0	1.5	207,349.5	1.5	1.340	1.237	1.061
557.294	11,444.1	3.5	190,882.5	4.5	0.900	0.813	0.954
557.590	22,919.6	3.5	202,263.2	4.5	0.303	0.267	0.165
557.732	40,202.6	1.5	219,500.4	1.5	0.254	0.266	0.206
558.528	24,028.4	4.5	203,069.9	3.5	0.094	0.269 *	0.095
558.833	16,772.4	0.5	195,716.1	1.5	0.608	0.476	0.523
560.257	28,859.8	0.5	207,349.5	1.5	0.513	0.449	0.537
560.695	37,019.4	4.5	215,369.6	4.5	0.698	0.489	0.885
561.057	24,028.4	4.5	202,263.2	4.5	0.179	0.250	0.080
561.828	32,155.8	5.5	210,146.1	5.5	0.310	0.321	0.249
562.123	14,678.3	4.5	192,575.6	3.5	0.652	0.808	0.682
562.374	27,894.0	1.5	205,711.8	1.5	1.400	1.164	1.523
562.550	39,600.8	2.5	217,361.9	1.5	0.877	0.760	0.641
562.880	14,430.2	1.5	192,087.9	0.5	0.752	0.756	0.866
562.950	6397.4	2.5	184,033.0	2.5	2.000	1.898	2.145
563.407	16,772.4	0.5	194,263.2	1.5	0.293	0.218	0.408
564.282	34,417.8	2.5	211,634.7	1.5	0.068	0.056	0.112
564.465	40,202.6	1.5	217,361.9	1.5	0.397	0.334	0.425
564.695	14,430.2	1.5	191,516.9	2.5	0.209	0.222	0.303
565.448	28,859.8	0.5	205,711.8	1.5	0.696	0.668	0.628
565.524	27,894.0	1.5	204,720.9	2.5	0.881	0.762	0.782
565.625	39,600.8	2.5	216,397.1	2.5	0.021	0.014 *	0.012 **
565.919	59,910.8	1.5	236,614.5	0.5	1.780	1.641	1.729
566.387	14,430.2	1.5	190,987.8	1.5	0.343	0.302	0.367
567.352	40,447.0	3.5	216,704.6	3.5	1.920	1.894	1.631
567.522	14,678.3	4.5	190,882.5	4.5	2.580	2.354	2.380
567.916	6397.4	2.5	182,479.5	3.5	0.853	0.759	0.858
568.343	40,447.0	3.5	216,397.1	2.5	0.127	0.202	0.173
568.698	0.0	1.5	175,839.8	1.5	2.420	2.233	2.477
570.000	34,417.8	2.5	209,856.0	3.5	0.550	0.445	0.443
570.398	16,772.4	0.5	192,087.9	0.5	0.077	0.091	0.076

Table 2. *Cont.*

λ (Å) [1]	Lower Level [2]		Upper Level [2]		gA (10^{10} s^{-1})		
	E (cm^{-1})	J	E (cm^{-1})	J	Previous [3]	HFR+CPOL [4]	MCDHF [4]
571.674	40,447.0	3.5	215,369.6	4.5	0.221	0.118 *	0.071
572.123	39,600.8	2.5	214,387.4	2.5	0.127	0.137	0.064
573.395	32,155.8	5.5	206,555.3	4.5	1.590	1.900	1.534
574.005	16,772.4	0.5	190,987.8	1.5	0.567	0.627	0.510
574.102	40,202.6	1.5	214,387.4	2.5	0.648	0.655	0.743
574.909	40,447.0	3.5	214,387.4	2.5	0.743	0.594	0.423
577.176	59,910.8	1.5	233,168.5	2.5	0.611	0.519	0.701
577.256	22,919.6	3.5	196,152.8	2.5	0.532	0.541	0.768
577.615	37,019.4	4.5	210,146.1	5.5	0.060	0.059	0.050 **
577.679	24,028.4	4.5	197,134.0	3.5	0.505	0.584	1.002
578.313	34,417.8	2.5	207,333.9	2.5	0.300	0.222	0.404
578.587	37,019.4	4.5	209,856.0	3.5	0.038	0.068 *	0.125
579.963	14,430.2	1.5	186,854.0	0.5	0.029	0.039 *	0.036
580.367	24,828.5	2.5	197,134.0	3.5	0.437	0.271	0.387
580.846	61,005.3	2.5	233,168.5	2.5	1.640	1.574	1.346
581.097	59,910.8	1.5	231,998.6	1.5	0.548	0.468	0.475
581.288	39,600.8	2.5	211,634.7	1.5	0.050	0.053 *	0.040
582.154	34,417.8	2.5	206,193.4	3.5	0.565	0.502	0.657
583.320	40,202.6	1.5	211,634.7	1.5	0.042	0.038 *	0.051
583.687	24,828.5	2.5	196,152.8	2.5	0.291	0.232	0.286
583.789	34,417.8	2.5	205,711.8	1.5	0.584	0.539	0.670
584.673	11,444.1	3.5	182,479.5	3.5	0.231	0.175	0.190
584.818	61,005.3	2.5	231,998.6	1.5	1.500	1.263	1.351
585.178	24,828.5	2.5	195,716.1	1.5	0.620	0.454	0.581
586.602	0.0	1.5	170,473.6	2.5	0.549	0.506	0.554
587.188	34,417.8	2.5	204,720.9	2.5	0.152	0.167	0.072
587.361	39,600.8	2.5	209,856.0	3.5	0.121	0.060 *	0.113
587.866	32,155.8	5.5	202,263.2	4.5	0.022	0.047 *	0.038
587.954	16,772.4	0.5	186,854.0	0.5	0.122	0.089	0.140
589.432	22,919.6	3.5	192,575.6	3.5	0.037	0.044 *	0.056
589.611	14,430.2	1.5	184,033.0	2.5	0.925	0.863	0.923
590.172	6397.4	2.5	175,839.8	1.5	0.014	0.008 *	0.015 **
590.286	40,447.0	3.5	209,856.0	3.5	0.111	0.061 *	0.094
591.104	37,019.4	4.5	206,193.4	3.5	0.368	0.297 *	0.503
593.126	22,919.6	3.5	191,516.9	2.5	0.049	0.094 *	0.021
595.148	59,910.8	1.5	227,935.6	2.5	0.705	0.609	0.498
595.942	14,678.3	4.5	182,479.5	3.5	0.343	0.370	0.320
596.136	24,828.5	2.5	192,575.6	3.5	1.090	1.006	1.056
596.188	39,600.8	2.5	207,333.9	2.5	0.575	0.560	0.473
597.903	61,005.3	2.5	228,256.2	3.5	1.260	1.134	1.182

Table 2. *Cont.*

λ (Å) [1]	Lower Level [2]		Upper Level [2]		gA (10^{10} s^{-1})		
	E (cm^{-1})	J	E (cm^{-1})	J	Previous [3]	HFR+CPOL [4]	MCDHF [4]
599.206	40,447.0	3.5	207,333.9	2.5	0.192	0.162	0.275
599.325	24,028.4	4.5	190,882.5	4.5	0.028	0.036 *	0.100
599.927	24,828.5	2.5	191,516.9	2.5	0.031	0.041	0.013
600.264	39,600.8	2.5	206,193.4	3.5	0.249	0.118	0.477
601.066	27,894.0	1.5	194,263.2	1.5	0.047	0.041 *	0.050
601.826	24,828.5	2.5	190,987.8	1.5	0.045	0.042 *	0.033
602.006	39,600.8	2.5	205,711.8	1.5	0.060	0.059	0.042
602.225	37,019.4	4.5	203,069.9	3.5	0.027	0.055 *	0.014
603.331	40,447.0	3.5	206,193.4	3.5	0.317	0.308	0.309
604.200	40,202.6	1.5	205,711.8	1.5	0.031	0.022 *	0.031
604.580	28,859.8	0.5	194,263.2	1.5	0.051	0.056	0.071
605.160	37,019.4	4.5	202,263.2	4.5	0.035	0.023 *	0.059
606.743	61,005.3	2.5	225,818.9	3.5	0.229	0.080 *	0.072
607.834	40,202.6	1.5	204,720.9	2.5	0.345	0.332	0.354
608.738	40,447.0	3.5	204,720.9	2.5	0.318	0.370	0.254
609.409	59,910.8	1.5	224,004.9	0.5	0.114	0.081 *	0.171
611.164	27,894.0	1.5	191,516.9	2.5	0.083	0.078	0.090
611.734	39,600.8	2.5	203,069.9	3.5	0.721	0.691	0.377
612.637	28,859.8	0.5	192,087.9	0.5	0.076	0.064	0.102
614.914	40,447.0	3.5	203,069.9	3.5	0.022	0.020 *	0.014 **
616.793	28,859.8	0.5	190,987.8	1.5	0.114	0.099	0.138
617.982	40,447.0	3.5	202,263.2	4.5	0.161	0.142	0.121 **
619.542	14,430.2	1.5	175,839.8	1.5	0.150	0.140	0.174
621.766	59,910.8	1.5	220,744.9	2.5	0.173	0.140	0.090
624.732	59,910.8	1.5	219,979.0	0.5	0.151	0.154	0.090
626.020	61,005.3	2.5	220,744.9	2.5	0.299	0.249	0.278
626.604	59,910.8	1.5	219,500.4	1.5	0.190	0.161	0.140
626.728	22,919.6	3.5	182,479.5	3.5	0.057	0.051	0.063
628.126	24,828.5	2.5	184,033.0	2.5	0.096	0.093	0.103
628.665	16,772.4	0.5	175,839.8	1.5	0.049	0.042	0.060
628.813	11,444.1	3.5	170,473.6	2.5	0.018	0.016 *	0.019
630.014	32,155.8	5.5	190,882.5	4.5	0.199	0.256	0.325
630.939	61,005.3	2.5	219,500.4	1.5	0.089	0.072 *	0.096
631.109	24,028.4	4.5	182,479.5	3.5	0.087	0.109	0.165
632.927	28,859.8	0.5	186,854.0	0.5	0.027	0.025	0.033
634.307	24,828.5	2.5	182,479.5	3.5	0.009	0.012	0.011
634.787	39,600.8	2.5	197,134.0	3.5	0.043	0.041	0.050 **
635.136	59,910.8	1.5	217,361.9	1.5	0.024	0.031 *	0.038
636.534	34,417.8	2.5	191,516.9	2.5	0.043	0.032 *	0.047
638.219	40,447.0	3.5	197,134.0	3.5	0.100	0.071	0.114

Table 2. *Cont.*

λ (Å) [1]	Lower Level [2]		Upper Level [2]		gA (10^{10} s^{-1})		
	E (cm^{-1})	J	E (cm^{-1})	J	Previous [3]	HFR+CPOL [4]	MCDHF [4]
638.698	34,417.8	2.5	190,987.8	1.5	0.070	0.062	0.087
638.764	39,600.8	2.5	196,152.8	2.5	0.175	0.159	0.170
639.568	61,005.3	2.5	217,361.9	1.5	0.034	0.032 *	0.039
640.549	39,600.8	2.5	195,716.1	1.5	0.124	0.138	0.156
640.848	14,430.2	1.5	170,473.6	2.5	0.052	0.051	0.063
646.570	39,600.8	2.5	194,263.2	1.5	0.023	0.027 *	0.016
647.344	59,910.8	1.5	214,387.4	2.5	0.016	0.012 *	0.012
649.097	40,202.6	1.5	194,263.2	1.5	0.006	0.004 *	0.004
649.931	37,019.4	4.5	190,882.5	4.5	0.078	0.072 *	0.085
658.393	40,202.6	1.5	192,087.9	0.5	0.040	0.037	0.055
661.943	40,447.0	3.5	191,516.9	2.5	0.009	0.014 *	0.008
664.738	40,447.0	3.5	190,882.5	4.5	0.048	0.038	0.043 **
668.385	34,417.8	2.5	184,033.0	2.5	0.046	0.039 *	0.058
675.399	34,417.8	2.5	182,479.5	3.5	0.019	0.014 *	0.017 **
686.606	24,828.5	2.5	170,473.6	2.5	0.005	0.005 *	0.005
695.257	40,202.6	1.5	184,033.0	2.5	0.011	0.011 *	0.015
696.443	40,447.0	3.5	184,033.0	2.5	0.016	0.011 *	0.016
701.360	27,894.0	1.5	170,473.6	2.5	0.029	0.025	0.032
704.066	40,447.0	3.5	182,479.5	3.5	0.031	0.029	0.037
764.104	39,600.8	2.5	170,473.6	2.5	0.025	0.022	0.028
823.207	61,005.3	2.5	182,479.5	3.5	0.007	0.007 *	0.006
940.059	100,973.9	2.5	207,349.5	1.5	0.342	0.257	0.337
944.741	108,538.4	3.5	214,387.4	2.5	0.258	0.192	0.259
958.446	123,600.5	3.5	227,935.6	2.5	0.500	0.300	0.420
975.001	114,140.1	2.5	216,704.6	3.5	0.192	0.130	0.129
977.922	114,140.1	2.5	216,397.1	2.5	0.236	0.173	0.190
984.931	115,173.8	4.5	216,704.6	3.5	0.512	0.352	0.426
986.987	108,538.4	3.5	209,856.0	3.5	0.389	0.357	0.388
997.955	97,940.4	1.5	198,144.3	0.5	0.585	0.419	0.515
998.040	115,173.8	4.5	215,369.6	4.5	1.040	0.865	1.066
998.213	132,989.9	3.5	233,168.5	2.5	1.580	1.036	1.661
1012.199	108,538.4	3.5	207,333.9	2.5	0.143	0.155	0.113
1018.199	97,940.4	1.5	196,152.8	2.5	0.457	0.386	0.343
1018.614	138,441.2	1.5	236,614.5	0.5	0.166	0.122	0.141
1020.229	108,538.4	3.5	206,555.3	4.5	0.759	0.626	0.324
1021.475	118,499.8	1.5	216,397.1	2.5	1.360	0.884	1.236
1024.015	108,538.4	3.5	206,193.4	3.5	0.306	0.282	0.053
1026.422	123,318.6	1.5	220,744.9	2.5	0.583	0.394	0.589
1026.617	130,849.6	4.5	228,256.2	3.5	1.120	0.730	1.187
1028.050	114,363.2	0.5	211,634.7	1.5	0.792	0.555	0.769

Table 2. *Cont.*

λ (Å) [1]	Lower Level [2]		Upper Level [2]		gA (10^{10} s^{-1})		
	E (cm^{-1})	J	E (cm^{-1})	J	Previous [3]	HFR+CPOL [4]	MCDHF [4]
1029.397	123,600.5	3.5	220,744.9	2.5	0.714	0.403	0.478
1034.565	123,318.6	1.5	219,979.0	0.5	0.253	0.178	0.237
1035.410	131,676.2	2.5	228,256.2	3.5	0.573	0.268	0.333
1038.184	97,940.4	1.5	194,263.2	1.5	0.838	0.612	0.833
1038.864	131,676.2	2.5	227,935.6	2.5	0.662	0.421	0.630
1039.709	123,318.6	1.5	219,500.0	1.5	0.203	0.076	0.051
1039.943	100,973.9	2.5	197,134.0	3.5	1.500	1.135	1.435 **
1047.439	130,849.6	4.5	226,320.5	5.5	3.760	2.574	3.576 **
1049.695	132,989.9	3.5	228,256.2	3.5	0.833	0.689	0.945
1050.652	100,973.9	2.5	196,152.8	2.5	0.568	0.470	0.507
1052.939	115,173.8	4.5	210,146.1	5.5	3.670	2.639	3.612 **
1053.231	132,989.9	3.5	227,935.6	2.5	0.276	0.185	0.167
1054.694	157,388.9	0.5	252,203.4	1.5	1.190	0.799	1.177
1055.665	138,441.2	1.5	233,168.5	2.5	0.327	0.182	0.200
1056.151	115,173.8	4.5	209,856.0	3.5	0.345	0.244	0.403
1057.849	108,538.4	3.5	203,069.9	3.5	0.483	0.260	0.726
1062.219	131,676.2	2.5	225,818.9	3.5	1.730	1.385	1.944 **
1063.333	123,318.6	1.5	217,361.9	1.5	0.733	0.464	0.742
1066.956	108,538.4	3.5	202,263.2	4.5	1.890	1.293	2.232 **
1068.531	118,499.8	1.5	212,086.5	0.5	0.335	0.238	0.333
1068.647	97,940.4	1.5	191,516.9	2.5	0.382	0.225	0.477 **
1068.864	138,441.2	1.5	231,998.6	1.5	1.140	0.670	1.028
1071.936	100,973.9	2.5	194,263.2	1.5	0.138	0.085	0.126
1072.848	114,140.1	2.5	207,349.5	1.5	0.603	0.410	0.569
1074.069	123,600.5	3.5	216,704.6	3.5	0.471	0.395	0.436
1075.424	114,363.2	0.5	207,349.5	1.5	0.102	0.082	0.102
1077.246	132,989.9	3.5	225,818.9	3.5	0.501	0.283	0.341
1086.336	114,140.1	2.5	206,193.4	3.5	1.030	0.744	0.605 **
1089.694	123,600.5	3.5	215,369.6	4.5	1.510	1.058	1.418 **
1094.314	115,173.8	4.5	206,555.3	4.5	0.490	0.323	0.482
1098.083	123,318.6	1.5	214,387.4	2.5	0.276	0.202	0.231
1098.651	115,173.8	4.5	206,193.4	3.5	0.012	0.011 *	0.019
1101.487	123,600.5	3.5	214,387.4	2.5	0.517	0.359	0.578
1103.982	114,140.1	2.5	204,720.9	2.5	0.366	0.188	0.482
1104.445	100,973.9	2.5	191,516.9	2.5	0.237	0.125	0.316
1117.393	138,441.2	1.5	227,935.6	2.5	0.387	0.271	0.478
1122.731	131,676.2	2.5	220,744.9	2.5	0.343	0.231	0.414
1124.334	132,989.9	3.5	221,932.2	4.5	1.320	0.948	1.365 **
1124.487	114,140.1	2.5	203,069.9	3.5	0.146	0.069	0.532 **
1126.533	123,318.6	1.5	212,086.5	0.5	0.119	0.092	0.126

Table 2. *Cont.*

λ (Å) [1]	Lower Level [2]		Upper Level [2]		gA (10^{10} s^{-1})		
	E (cm^{-1})	J	E (cm^{-1})	J	Previous [3]	HFR+CPOL [4]	MCDHF [4]
1141.380	108,538.4	3.5	196,152.8	2.5	0.103	0.052	0.140
1183.150	130,849.6	4.5	215,369.6	4.5	0.146	0.107	0.132
1213.899	132,989.9	3.5	215,369.6	4.5	0.218	0.084	0.192 **
1214.431	108,538.4	3.5	190,882.5	4.5	0.242	0.191	0.330 **
1226.917	100,973.9	2.5	182,479.5	3.5	0.416	0.319	0.487 **
1262.213	157,388.9	0.5	236,614.5	0.5	0.239	0.153	0.255 **
1283.719	97,940.4	1.5	175,839.8	1.5	0.181	0.125	0.197
1291.962	1151,73.8	4.5	192,575.6	3.5	0.747	0.563	0.818
1292.383	1141,40.1	2.5	191,516.9	2.5	0.117	0.081	0.133
1320.854	1151,73.8	4.5	190,882.5	4.5	0.774	0.566	0.861
1324.610	1085,38.4	3.5	184,033.0	2.5	0.516	0.388	0.565
1350.694	1316,76.2	2.5	205,711.8	1.5	0.416	0.320	0.471
1352.428	1085,38.4	3.5	182,479.5	3.5	0.472	0.338	0.501
1366.055	1329,89.9	3.5	206,193.4	3.5	0.162	0.088	0.315
1378.678	97,940.4	1.5	170,473.6	2.5	0.451	0.341	0.501 **
1381.265	123,318.6	1.5	195,716.1	1.5	0.100	0.070	0.088
1426.942	132,989.9	3.5	203,069.9	3.5	0.205	0.215	0.148
1430.758	114,140.1	2.5	184,033.0	2.5	0.180	0.129	0.193
1443.568	132,989.9	3.5	202,263.2	4.5	0.085	0.072	0.028 **
1449.783	123,600.5	3.5	192,575.6	3.5	0.253	0.199	0.262
1451.520	138,441.2	1.5	207,333.9	2.5	0.111	0.060	0.162 **
1463.294	114,140.1	2.5	182,479.5	3.5	0.216	0.158	0.216 **
1466.297	123,318.6	1.5	191,516.9	2.5	0.114	0.097	0.113 **
1486.275	123,600.5	3.5	190,882.5	4.5	0.357	0.256	0.346 **

[1] Experimental wavelengths from [6]. [2] Experimental energy levels from [6,7]. [3] Calculated transition probabilities from [6]. [4] Calculated transition probabilities obtained in the present work. gA-values with * symbol correspond to transitions for which $CF < 0.05$ in HFR+CPOL calculations, while gA-values with ** symbol correspond to transitions for which $dT > 0.25$ in MCDHF calculations (see text).

A first observation that can be made when looking at this table is that our HFR+CPOL transition probabilities are in good agreement with the results previously published by Raassen et al. [6], with a mean ratio $gA_{\mathrm{HFR+CPOL}}/gA_{\mathrm{Raassen}}$ equal to 0.95 $\pm$ 0.21 (where the number after $\pm$ represents the standard deviation from the mean), which is quite comparable to the ratio we get when comparing our HFR calculations with and without core polarization corrections, i.e., $gA_{\mathrm{HFR+CPOL}}/gA_{\mathrm{HFR}}$ = 0.98 $\pm$ 0.10. It should be noted, however, that our new HFR+CPOL results were obtained on the basis of a more extensive configuration interaction model than the one considered in [6].

It is also interesting to note that the agreement between the HFR+CPOL and MCDHF results obtained in the present work is generally good, the mean ratio between both sets of data, $gA_{\mathrm{HFR+CPOL}}/gA_{\mathrm{MCDHF}}$, being equal to 1.08 $\pm$ 0.42, if we exclude the two transitions at 526.999 and 555.333 Å for which the gA-values differ from each other by one or two orders of magnitude. This means that the majority of our gA-values calculated using the two methods agree within a few tens of percent. Such a comparison is shown in Figure 2 where transition probabilities obtained using the HFR+CPOL approach are plotted against those deduced from MCDHF calculations.

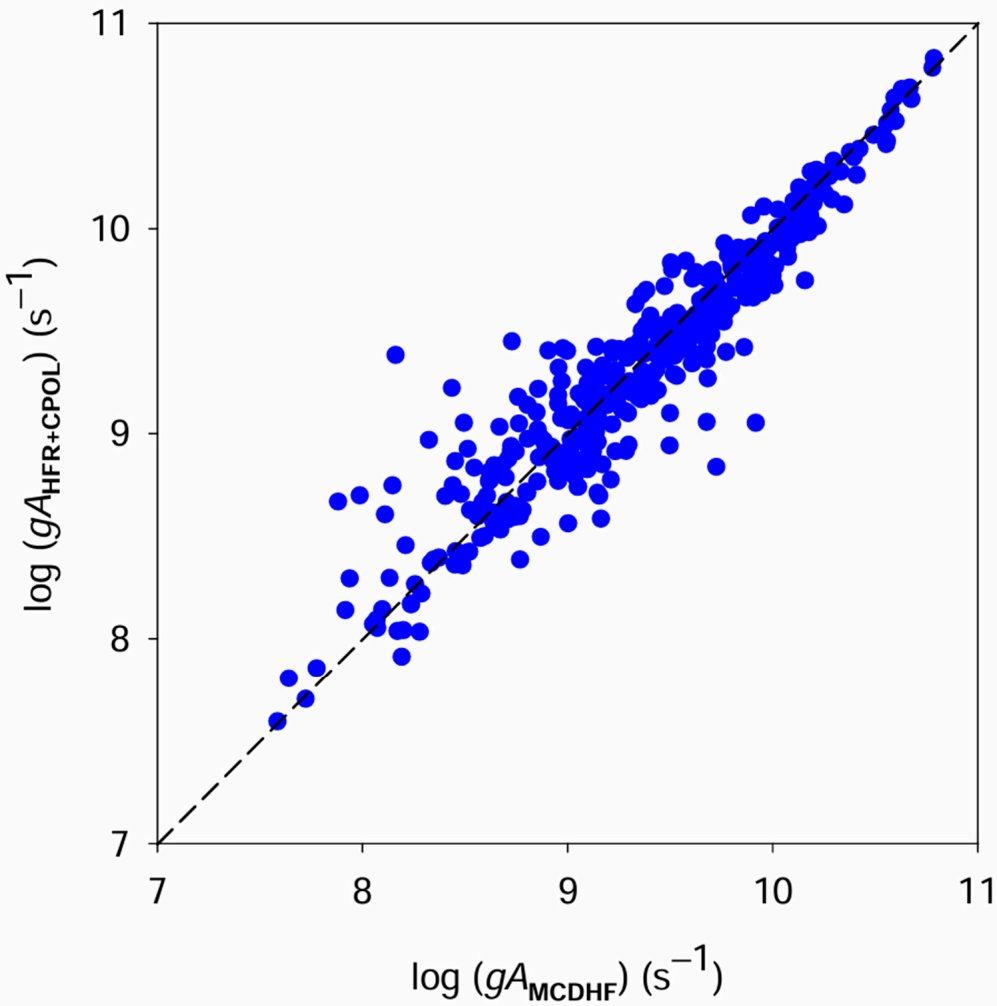


Figure 2. Comparison between transition probabilities (gA) obtained using the HFR+CPOL method and those deduced from MCDHF calculations for all Os VI lines considered in the present work (blue dots).

The quality of the transition probabilities obtained in our work can also be estimated from parameters such as the cancellation factor (*CF*) and the uncertainty parameter (*dT*) for HFR+CPOL and MCDHF calculations, respectively. As a reminder, the former parameter is defined by [8]:

$$CF = \left[\frac{\left| \sum\sum y^{\gamma}_{\beta J} \left\langle \beta J \right\| P^{(1)} \left\| \beta\prime J\prime \right\rangle y^{\gamma\prime}_{\beta\prime J\prime} \right|}{\sum\sum \left| y^{\gamma}_{\beta J} \left\langle \beta J \right\| P^{(1)} \left\| \beta\prime J\prime \right\rangle \right| y^{\gamma\prime}_{\beta\prime J\prime} \right]^2 \quad (1)$$

where $P^{(1)}$ is the dipole operator for the transition between two atomic states $|\gamma J\rangle$ and $|\gamma' J'\rangle$ developed in terms of pure basis states $|\beta J\rangle$ and $|\beta' J'\rangle$, with $y^{\gamma}{}_{\beta J}$ and $y^{\gamma'}{}_{\beta' J'}$ as mixing coefficients, respectively. According to Cowan [8], very small values of this parameter (typically $CF < 0.05$) may be expected to show significant errors in the computed line strengths. In our work, it was verified that the *CF*-values were larger than 0.05 for most of the lines listed in Table 2, the only exceptions occurring for 91 transitions (among 367) generally characterized by rather weak gA-values (typically smaller than 10^9 s^{-1}). This is illustrated in Figure 3, where the *CF* parameter is plotted as a function of HFR+CPOL transition probabilities for all Os VI lines considered in the present work.

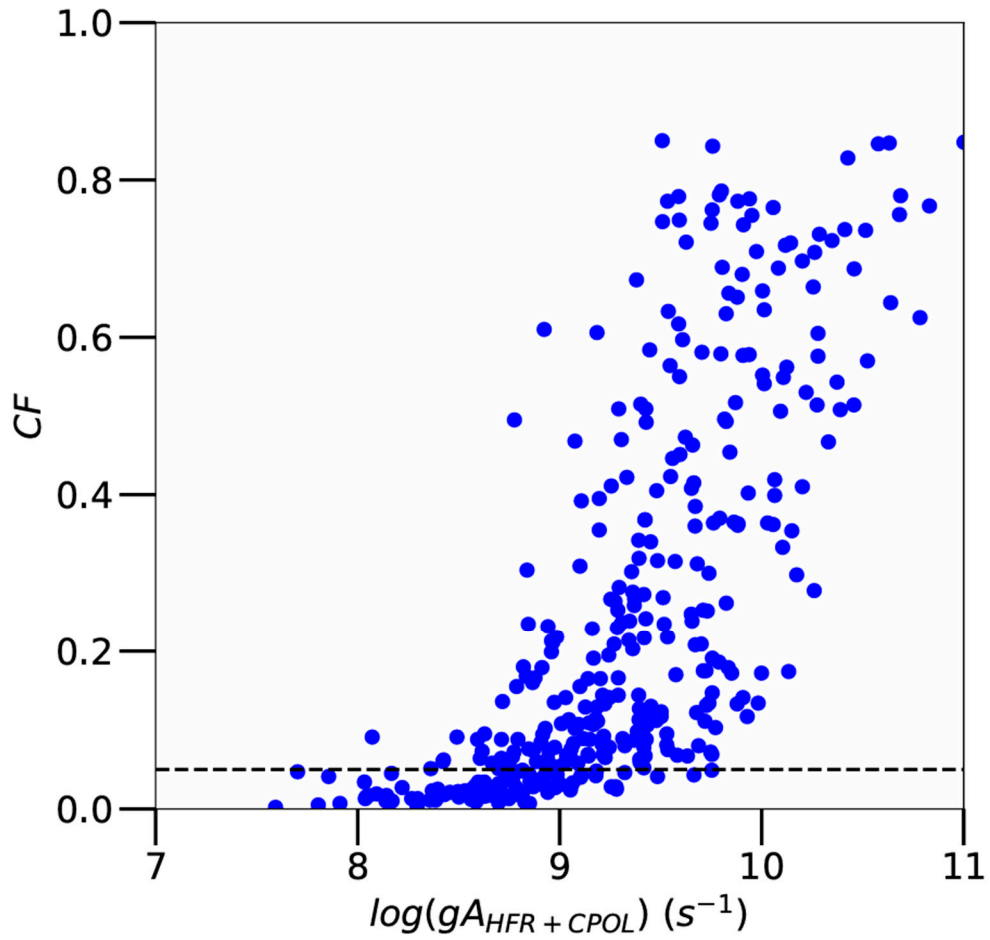


Figure 3. Cancellation factors (*CF*) as a function of gA-values obtained using the HFR+CPOL method for all Os VI transitions considered in the present work (blue dots). The dotted line corresponds to $CF = 0.05$.

As for the dT parameter, it is expressed by [17]:

$$dT = \frac{|A_B - A_C|}{\max(A_B, A_C)} \quad (2)$$

where A_B and A_C are transition probabilities in Babushkin (length) and Coulomb (velocity) gauges, the electric dipole transition moment having the same value in both formalisms for exact solutions of the Dirac equation [18]. The dT parameter thus provides a statistical estimate of the uncertainty of MCDHF transition rates for approximate solutions for which the transition moment differs from one gauge to another. For transitions listed in Table 2, the average value of dT was found to be equal to 0.17 ± 0.06, which means that the uncertainties affecting most or our MCDHF gA-values do not exceed 25%. The few exceptions for which the dT parameter was found to be greater than 25% concern only 42 transitions out of the 367 listed in Table 2. This is illustrated in Figure 4, where dT is plotted as a function of gA_{MCDHF}.

Finally, it should be noted that, if we set aside the transitions listed in Table 2, for which both $CF < 0.05$ (in the HFR+CPOL calculations) and $dT > 0.25$ (in the MCDHF calculations), there remain 250 transitions whose differences between the gA-values obtained using the two methods do not exceed 30%, the mean relative deviation $\Delta gA/\langle gA\rangle$ (where $\Delta gA = |gA_{\mathrm{HFR+CPOL}} - gA_{\mathrm{MCDHF}}|$ and $\langle gA\rangle = (gA_{\mathrm{HFR+CPOL}} + gA_{\mathrm{MCDHF}})/2$) being equal to 0.29. Consequently, at least for these 250 lines, the uncertainty on the HFR+CPOL and MCDHF transition probabilities obtained in our work can be estimated at most 30%, the

gA-values of other transitions can be affected by slightly larger uncertainties up to a factor of two. However, given the much better agreement obtained between the HFR+CPOL energy levels and the experimental values, we can assume that the $gA_{\mathrm{HFR+CPOL}}$-values are of better quality overall than the MCDHF results.

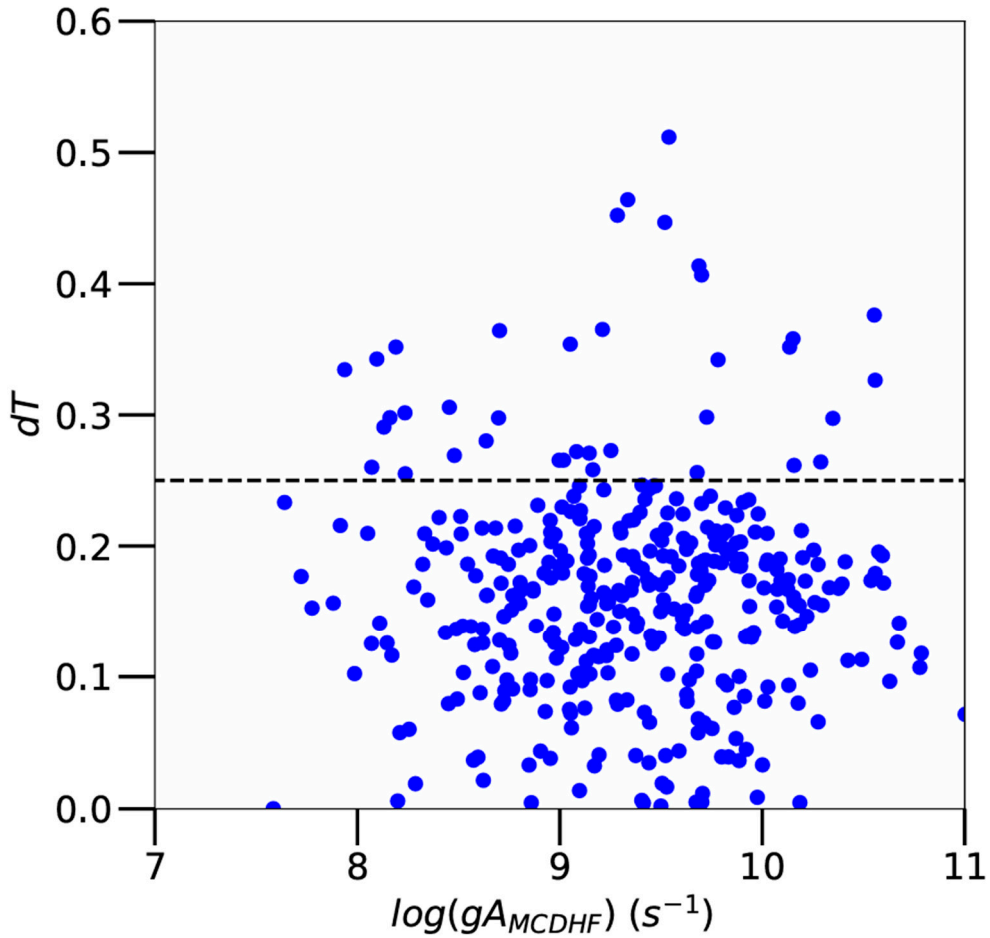


Figure 4. Uncertainty parameter (dT) as a function of gA-values obtained using the MCDHF method for all Os VI transitions considered in the present work (blue dots). The dotted line corresponds to $dT = 0.25$.

4. Conclusions

New transition probabilities for experimentally observed lines in the Os VI spectrum are reported in the present work. They were obtained using two different computational approaches based on the pseudo-relativistic Hartree–Fock method including core polarization corrections (HFR+CPOL) and the fully relativistic Multiconfiguration Dirac–Hartree–Fock method (MCDHF). Based on the detailed comparison showing a good agreement between the two sets of results (within a few tens of percent for most transitions), it can be concluded that the $gA_{\mathrm{HFR+CPOL}}$-values reported in this paper for Os VI lines can be considered to be of fairly good quality for their application in plasma diagnostics. These new atomic data will thus be useful for the analysis of the spectra emitted by fusion plasmas produced in Tokamaks such as ITER.

Author Contributions: Conceptualization, M.B. and P.Q.; methodology, M.B., P.P. and P.Q.; software, M.B.; validation, M.B., P.P. and P.Q.; formal analysis, M.B.; investigation, M.B.; resources, M.B. and P.Q.; data curation, M.B. and P.Q.; writing—original draft preparation, P.Q.; writing—review and editing, M.B., P.P. and P.Q.; visualization, P.Q.; supervision, P.Q.; project administration, P.Q.; funding acquisition, P.P. and P.Q. All authors have read and agreed to the published version of the manuscript.

Funding: This research was funded by F.R.S.-FNRS—EOS grant number O.0004.22.

Data Availability Statement: The original contributions presented in this study are included in the article.

Acknowledgments: P.P. and P.Q. are, respectively, Research Associate and Research Director of the Belgian Fund for Scientific Research F.R.S.-FNRS. This project received funding from the FWO and F.R.S.-FNRS under the Excellence of Science (EOS) program (number O.0004.22). Part of the atomic calculations were made with computational resources provided by the Consortium des Equipements de Calcul Intensif (CECI), funded by the F.R.S.-FNRS under grant no. 2.5020.11 and by the Walloon Region of Belgium.

Conflicts of Interest: The authors declare no conflicts of interest.

References

1. Pitts, R.A.; Carpentier, S.; Escourbiac, F.; Hirai, T.; Komarov, V.; Lisgo, S.; Kukushkin, A.S.; Merola, M.; Sashala Naik, A.; Mitteau, R.; et al. A full tungsten divertor for ITER: Physics issues and design status. *J. Nucl. Mater.* **2013**, *438*, S48. [CrossRef]
2. Hirai, T.; Panayotis, S.; Barabash, V.; Amzallag, C.; Escourbiac, F.; Durocher, A.; Merola, M.; Linke, J.; Loewenhoff, T.; Pintsuk, G.; et al. Use of tungsten material for the ITER divertor. *Nucl. Mat. En.* **2016**, *9*, 616. [CrossRef]
3. Pitts, R.A.; Bonnin, X.; Escourbiaca, F.; Frerichs, H.; Gunn, J.P.; Hirai, T.; Kukushkin, A.S.; Kaveeva, E.; Miller, M.A.; Moulton, D.; et al. Physics basis for the first ITER tungsten divertor. *Nucl. Mat. En.* **2019**, *20*, 100696. [CrossRef]
4. Gilbert, N.R.; Sublet, J.C. Neutron-induced transmutation effects in W and W-alloys in a fusion environment. *Nucl. Fusion* **2011**, *51*, 043005. [CrossRef]
5. Kunze, H.-J. *Introduction to Plasma Spectroscopy*; Springer: Berlin/Heidelberg, Germany, 2009.
6. Raassen, A.J.J.; Azarov, V.I.; Uylings, P.H.M.; Joshi, Y.N.; Tchang-Brillet, L.; Ryabtsev, A.N. Analysis of the spectrum of five times ionized osmium (Os VI). *Phys. Scr.* **1996**, *54*, 56. [CrossRef]
7. Azarov, V.I. Parametric study of the $5d^3$, $5d^26s$ and $5d^26p$ configurations in the Lu I isoelectronic sequence (Ta III–Hg X) using orthogonal operators. *At. Data Nucl. Data Tables* **2018**, *119*, 193. [CrossRef]
8. Cowan, R.D. *The Theory of Atomic Structure and Spectra*; University of California Press: Berkeley, CA, USA, 1981.
9. Quinet, P.; Palmeri, P.; Biémont, E.; McCurdy, M.M.; Rieger, G.; Pinnington, E.H.; Wickliffe, M.E.; Lawler, J.E. Experimental and theoretical lifetimes, branching fractions and oscillator strengths in Lu II. *Mon. Not. R. Astron. Soc.* **1999**, *307*, 934. [CrossRef]
10. Quinet, P.; Palmeri, P.; Biémont, E.; Li, Z.S.; Zhang, Z.G.; Svanberg, S. Radiative lifetime measurements and transition probability calculations in lanthanide ions. *J. Alloys Compd.* **2002**, *344*, 255. [CrossRef]
11. Quinet, P. Overview of recent advances performed in the study of atomic structures and radiative processes for the lowest ionization stages of heavy elements. *Can. J. Phys.* **2017**, *95*, 790. [CrossRef]
12. Brasseur, M.; Gamrath, S.; Quinet, P. Radiative decay rates for electric dipole transitions in doubly-, trebly- and quadruply-charged rhenium ions(Re III–V) of interest to nuclear fusion research and astrophysical spectra analyses. *At. Data Nucl. Data Tables* **2024**, *157*, 101636. [CrossRef]
13. Fraga, S.; Karwowski, J.; Saxena, K.M.S. *Handbook of Atomic Data*; Elsevier: Amsterdam, The Netherlands, 1976.
14. Grant, I.P. *Relativistic Quantum Theory of Atoms and Molecules*; Springer: New York, NY, USA, 2007.
15. Froese Fischer, C.; Godefroid, M.R.; Brage, T.; Jönsson, P.; Gaigalas, G. Advanced multiconfiguration methods for complex atoms: I. Energies and wave functions. *J. Phys. B At. Mol. Opt. Phys.* **2016**, *49*, 182004. [CrossRef]
16. Froese Fischer, C.; Gaigalas, G.; Jönsson, P. GRASP2018—A Fortran 95 version of the General Relativistic Atomic Structure Package. *Comput. Phys. Commun.* **2019**, *237*, 184. [CrossRef]
17. Ekman, J.; Godefroid, M.R.; Hartman, H. Validation and implementation of uncertainty estimates of calculated transition Rates. *Atoms* **2014**, *2*, 215. [CrossRef]
18. Grant, I.P. Gauge invariance and relativistic radiative transitions. *J. Phys. B* **1974**, *7*, 1458. [CrossRef]

Disclaimer/Publisher's Note: The statements, opinions and data contained in all publications are solely those of the individual author(s) and contributor(s) and not of MDPI and/or the editor(s). MDPI and/or the editor(s) disclaim responsibility for any injury to people or property resulting from any ideas, methods, instructions or products referred to in the content.